Kusche, J., Schmidt, R., Petrovic, S., Rietbroek, R. (2009): Decorrelated GRACE time-variable gravity solutions by GFZ, and their validation using a hydrological model. - Journal of Geodesy, 83, 10, 903-913

DOI: 10.1007/s00190-009-0308-3

Decorrelated GRACE Time-Variable Gravity Solutions by GFZ, and their Validation using a Hydrological Model

J. Kusche,[1] R. Schmidt,[1,2] S. Petrovic,[1] and R. Rietbroek[1]

J. Kusche, GFZ Potsdam, Telegrafenberg, 14473 Potsdam, Germany (jkusche@gfz-potsdam.de)

[1]GeoForschungsZentrum Potsdam,

Germany.

[2]Now at: Astrium GmbH,

Robert-Koch-Str. 1,81633 München,

Germany.

Abstract. We have analyzed recent GRACE RL04 monthly gravity solutions, using a new decorrelating post-processing approach. We find very good agreement with mass anomalies derived from a global hydrological model (WGHM). The post-processed GRACE solutions exhibit only little amplitude damping and an almost negligeable phase shift and period distortion for relevant hydrological basins. Furthermore, these post-processed GRACE solutions have been inspected in terms of data fit with respect to the original inter-satellite ranging and to SLR and GPS observations. This kind of comparison is new. We find variations of the data fit due to solution post-processing only within very narrow limits. This confirms our suspicion that GRACE data does not firmly 'pinpoint' the standard unconstrained solutions. Regarding the original Kusche (2007) decorrelation and smoothing method, a simplified (order-convolution) approach has been developed. This simplified approach allows to realize a higher resolution – as necessary e.g. for generating computed GRACE observations – and needs far less coefficients to be stored.

1. Introduction

Using data provided by the Gravity Recovery and Climate Experiment (GRACE) twin-satellite mission (Tapley et al., 2004b), scientists from various diciplines have been able, for the first time, to observe directly the redistribution of mass in the world's ocean (e.g. Chambers et al., 2004), the mass balance of the Greenland and Antarctica ice sheets (e.g. Velicogna and Wahr, 2004), water stock changes in the Amazon and many other areas (e.g. Schmidt et al., 2006), and the co- and post-seismic gravity effect associated with large seismic events such as the December 2004 Sumatra-Andaman Earthquake (Han and Simons, 2008).

However, one significant problem that users of monthly GRACE gravity field solutions face is the presence of correlated and resolution-dependent noise in the provided spherical harmonic coefficients. Simply truncating the spherical harmonic series at low degrees (long wavelengths), where the noise is not yet significant, causes the loss of an unacceptably large portion of the signal. This is not an option when one is interested in signals of geographical extension of a few hundred kilometers, such as in the case of e.g. smaller ocean basins (Fenoglio-Marc et al., 2006, Swenson and Wahr, 2007) or geodynamic phenomena (Han and Simons, 2008). The noise is not white on the sphere, and its realization is usually described as 'striping' patterns. The reason for this peculiar characteristics is GRACE's mission geometry in connection with potential limitations in current analysis strategies. The GRACE A and B twin-satellites fly in a single orbital plane, and the inter-satellite ranging observable used in gravity modelling translates into a distinct along-track sensitivity. Deficiencies in de-aliasing background models and other errors

and mismodelling then yield an anisotropic error pattern.

Gaussian smoothing (convolution against an isotropic Gaussian smoothing kernel) has been the standard method in the early exploitation of GRACE products, due to its ease in implementation and intuitive interpretation (Wahr et al., 1998). However, more recent works tend to apply probabilistic decorrelation methods in the post-processing of GRACE solutions, usually in conjunction with an additional smoothing. The idea behind the decorrelation is to identify and remove error correlation in the sets of spherical harmonic coefficients (i.e. between different coefficients), either based on empirical analysis of the coefficients (Swenson and Wahr 2006, Wouters and Schrama, 2007) or using an *a priori* synthetic model of the observation geometry (Kusche 2007, Klees et al., 2008). As a consequence the resulting decorrelating kernels, unlike the original Gaussian or some modified versions of it, are not axisymmetric (isotropic); they rather tend to exhibit negative sidelobes in North-South direction, and their overall shape depends on the geographical position. We believe that this kind of investigation will continue for the near future, unless the quality of the GRACE gravity models experiences a quantum leap rather than steady progress, which is not foreseeable at the moment.

The objectives of the present paper are as follows. First, we simplify and extend the Kusche (2007) decorrelation method to facilitate its usage by a wider community of users of GRACE-derived products. Second, we decorrelate the GFZ GRACE RL04 series (Flechtner, 2007, Schmidt et al., 2008b) of monthly gravity field solutions. Finally, these decorrelated solutions are evaluated and compared to predictions from a hydrological model.

The Kusche (2007) method was originally based on computing and applying a filter matrix with as many rows and columns as there are spherical harmonic coefficients. Now we simplify it to an order-only convolution method (comparable to the approach in Swenson and Wahr (2006)) which still closely complies with the original, statistically optimal, full-matrix method. These order convolution filter coefficients are provided to the scientific community for three different degrees of smoothness. In this manuscript we first briefly recap the decorrelation method of Kusche (2007) and then develop our simplified/extended version of it. These two approaches are compared in terms of complexity as well as in terms of absolute and relative differences of the filter coefficients. Then, we compare our decorrelated GFZ GRACE RL04 solutions first in terms of fit to the original K-band data and to SLR and GPS phase and code observations in the orbit recovery process. Furthermore, we investigate the stability of amplitudes, phases and periods of leading Empirical Orthogonal Functions (EOF's) for selected water catchment areas. Finally, we perform a global comparison with independent hydrological modelling.

2. Filter Method and Data

2.1. Approach

The unphysical striping error pattern, seen in typical monthly solutions of the GRACE project when geoid or surface mass anomaly maps are constructed, can be understood as an individual realization of a noise process with a spatially distinct correlation. This noise process affects predominantly the higher spherical harmonic degrees. Unlike deterministic smoothing kernels, probabilistic methods deal with this situation in a natural and optimal way when *a priori* signal and error covariance operators can be specified. This

is applied in the methods of Swenson and Wahr (2006), Kusche (2007), and Wouters and Schrama (2007). These methods differ only in the way how these covariance operators are constructed. Moreover, despite striving for optimality under specified signal and error metrics, these methods are usually being relaxed in the sense that additional smoothing is enabled through a continuous tuning parameter. In the case of Swenson and Wahr (2006), Gaussian smoothing is applied after decorrelation (where the covariance is constructed from an empirical inspection of the coefficients), and the degree of smoothing is further controlled by parameters that tune the polynomial covariance fit. Kusche (2007) applied a common concept from inverse theory: penalized weighted inversion, where the penalty (or regularization) parameter controls the desired degree of smoothness for the geoid or surface mass anomaly solution. Wouters and Schrama (2007) first apply empirical orthogonal function (EOF) analysis to the GRACE coefficients. Therafter, based on applying the Kolmogorov-Smirnov test to the principal components, signal and noise covariance are empirically separated and the smoothed and decorrelated signal is obtained from a partial reconstruction. Other authors (e.g. Davis et al., 2008) apply a simple trend/trigonometric polynomial models for each individual coefficient to this end.

In the Kusche (2007) method, the GRACE error covariance matrix used in the construction of the decorrelating kernel is created synthetically, using one month of GRACE twin-spacecraft orbits and a simplified method for mapping the K-band inter-satellite ranging observations into the spherical harmonics. This matrix models the resulting correlations between GRACE spherical harmonic coefficients quite well, and we found no need to replace it with a more realistic formal or calibrated GRACE error covariance from the level

2 processing. On the contrary, experiments indicated that the resulting kernels would exhibit a more complicated structure (e.g. more sidelobes, as expected) without providing any real advantages. The disadvantage of the Kusche (2007) method lies in the fact that a fully populated filter matrix is built: every filtered coefficient is computed as a weighted average of all n_K coefficients (cf. Eq. (4)). Swenson and Wahr (2006), on the other hand, derived their method as an order-convolution filter, i.e. a filtered spherical harmonic coefficient is constructed using only the coefficients of the same harmonic order and over the same parity. Why this is effective is not surprising: from its observing geometry, it is clear that GRACE (at least for good periods without larger data gaps) comes close to fulfilling certain sampling conditions (Colombo, 1986), for which the normal matrix would attain a special, block-diagonal structure.

2.2. Order convolution coefficients

In the Kusche (2007) method with smoothing parameter a, each spherical harmonic coefficient ($\sigma_{lmq} = c^{\sigma}_{lm}$ for $q = 0$ and $\sigma_{lmq} = s^{\sigma}_{lm}$ for $q = 1$) of the surface mass anomaly $\sigma(\lambda, \theta)$ (or any other functional of gravity change) is decorrelated and smoothed in the following way

$$\sigma^{\text{filt}}_{lmq} = \sum_{l'=l_{\min}}^{l_{\max}} \sum_{m'=0}^{l'} \sum_{q'=0}^{1} w^{l'm'q'}_{lmq}(a)\ \sigma_{l'm'q'} \tag{1}$$

Here l and m are harmonic degree and order, and the surface mass anomaly coefficients follow from published GRACE geopotential coefficients x_{lmq} (Wahr et al., 1998)

$$\sigma_{lmq} = \frac{2\rho_e}{3\rho_w(1+k'_l)}(l+\frac{1}{2})\delta x_{lmq}\ , \tag{2}$$

where ρ_e and ρ_w are average (reference) densities of Earth and sea-water, k'_l is the load Love number of degree l, $\delta x_{lmq} = x_{lmq} - \bar{x}_{lmq}$, and $\bar{x}_{lmq}$ is a long-time average of the geopotential coefficient. $l_{\min}$ and $l_{\max}$ are the minimum and maximum spherical harmonic degrees (usually $l_{\min} = 2$ and $l_{\max} = 40 \ldots 120$). $w_{lmq}^{l'm'q'}(a)$ is the matrix of decorrelation coefficients, with a continuous non-negative parameter a that controls the degree of smoothness. The reason for using a dense matrix, i.e. each coefficient $\sigma_{lmq}^{\text{filt}}$ following from a weighted mean of all other coefficients, is that the error covariance matrix $\mathbf{E}$ and the signal covariance matrix $\mathbf{S}$ will in general be given as dense matrices. Then, it follows straightforward from probabilistic inverse principles that

$$\mathbf{W}_a = (\mathbf{E}^{-1} + a\mathbf{S}^{-1})^{-1}\mathbf{E}^{-1} = \left(\mathbf{I} + (a - a')\mathbf{W}_{a'}\mathbf{E}\mathbf{S}^{-1}\right)\mathbf{W}_{a'} \ , \tag{3}$$

see Kusche (2007). There, it was also shown that this filter is equivalent to the common (quadratic) constraining of the GRACE solutions, if $\mathbf{E}^{-1}$ equals the GRACE normal equations matrix and $\mathbf{S}^{-1}$ equals the regularization matrix. Gaussian and other commonly used noise suppression methods employ a diagonal matrix, hence they cannot decorrelate the coefficients. The downside of the full-matrix approach is that the number of filter coefficients n_K is quite large,

$$n_K = \left((l_{\max} + 1)^2 - l_{\min}^2\right)^2 \ . \tag{4}$$

Table 1 provides an overview of the smoothing properties of the three filter versions (denoted by DDK1, DDK2, DDK3) that we evaluate in this paper, in terms of the smoothing radius of an approximately equivalent Gaussian filter. However, there are different possibilities to define a correspondence between an anisotropic filters (which possess negative sidelobes in our case) and an isotropic all-positive Gaussian. We provide two of them: 1)

based upon the assessment in Kusche (2007) which defines the spectral variance of the squared isotropic and anisotropic function thought as a probability distribution on the sphere, and 2) based on comparing the 'isotropic part' of the anisotropic decorrelation filter with the Gaussian in terms of matching the particular spectral degree where the filter weight drops to 0.5, i.e. by defining

$$\omega_l = \left(\frac{\sum_{m=0}^{l} \sum_{q=0}^{1} \left(w_{lmq}^{lmq}(a) \right)^2}{2l+1} \right)^{\frac{1}{2}} \quad . \tag{5}$$

In fact, Gaussian radii based on 1) and 2) differ significantly (cf. table 1). This is not surprising since method 2) completely disregards the anisotropic structure of the filter kernel, whereas in method 1) negative sidelobes map into positive ones and in this way artificially increase the variance.

Swenson and Wahr (2006) noted several approximate symmetry properties, including a strong correlation between even and odd parity as a function of degree, from empirical inspection of the correlations of the GRACE coefficients. We translate them here to the filter coefficients,

$$\begin{aligned}
&|w_{lm0}^{l'm'1}(a)| \ll 1 \\
&|w_{lm1}^{l'm'0}(a)| \ll 1 \\
&|w_{lmq}^{l'm'q'}(a)| \ll 1 \qquad \text{for} \qquad m \neq m' \\
&|w_{lmq}^{l'm'q'}(a)| \ll 1 \qquad \text{for} \qquad l \text{ even and } l' \text{ odd} \\
&|w_{lmq}^{l'm'q'}(a)| \ll 1 \qquad \text{for} \qquad l \text{ odd and } l' \text{ even} .
\end{aligned} \tag{6}$$

The reason for these symmetries is the dense, almost regular distribution of the satellite measurements along a near-circular, near-repeat orbit of almost constant inclination and

of sufficient number of orbital revolutions. Colombo (1986) showed that under such conditions the spectrum of the design matrix columns will be clustered at only few lines, and two columns will share common lines only for common harmonic order, same parity of degree, and for cos/cos and sin/sin combinations. Note that the spectral convolution coefficients themselves are not necessarily symmetric in the Kusche (2007) method, $w_{lmq}^{l'm'q'} \neq w_{l'm'q'}^{lmq}$, but they retain the general properties of the normal matrix since the signal covariance matrix was chosen as diagonal. In addition, from the mentioned conditions one readily derives

$$|w_{lm0}^{l'm'0}(a) - w_{lm1}^{l'm'1}(a)| \ll 1 \tag{7}$$

i.e. c_{lm} and s_{lm}-coefficients are filtered in the same way. We have investigated in table 2 (ESM) the maximum size of neglected coefficients, when assuming that Eq. (6) and Eq. (7) would be perfectly fulfilled (i.e. by replacing the left-hand side by zeroes). This comes down to a maximum contribution of 0.035 from mixed-parity coefficient pairs, and of up to 0.012 considering only the block-diagonality (i.e. by retaining only coefficients of the same order m). Admitting that the considered filters were based on the GRACE orbital geometry for August 2003, a month with a good spatial coverage of observations, we conclude that it appears perfectly justified to work with the block-diagonal filter as an approximation to the statistically optimal method (where optimality depends on *a priori* assumptions which can be challenged to some extent). A visual representation of the kernel cross-sections in North-South and East-West directions would be hard to distinguish from the figures 2-5 in Kusche (2007), derived from the optimal filter. Therefore, we omit such figures here. During the review phase of this paper, Klees et al. (2008) published an

extended set of experiments where both covariance matrices **E** and **S** are varied.

Assuming the above conditions (6) as exactly fulfilled, as inferred from Swenson and Wahr (2006), the decorrelation method can be written as

$$\sigma_{lmq}^{\text{filt}} = \sum_{l'=l_{\min};l'\in\text{parity}(l)}^{l_{\max}} w(l,l',m,a)\sigma_{l'mq} \ , \tag{8}$$

where $l' \in \text{parity}(l)$ means that we consider only those l' in order to form the sum which are of the same parity (both even or both odd) as l. The number of coefficients is now reduced from n_K to

$$\begin{aligned} n_k \ &= \ \frac{1}{2}(l_{\min}+1)(\Delta l+1)^2 + \frac{\Delta l}{12}(\Delta l+1)(2\Delta l+1) \\ &+ \ \frac{1}{4}(\Delta l+1) \\ &+ \ \left\{ \begin{matrix} 1 & \text{if parity}(\Delta l)=\text{even} \\ 0 & \text{if parity}(\Delta l)=\text{odd} \end{matrix} \right\} \times \frac{(2l_{\min}+1)}{4} \ , \end{aligned} \tag{9}$$

where

$$\Delta l = l_{\max} - l_{\min} \ . \tag{10}$$

For example, for $l_{\min} = 2$ and $l_{\max} = 70$ this gives $n_K = 5037^2 \approx 2.5 \cdot 10^7$, whereas we have $n_k = 60727 \approx 6.1 \cdot 10^4$, which means that a compression factor n_k/n_K of 0.0024 is achieved.

In addition, a threshold ε can be introduced to suppress coefficients of negligible magnitude. In table 3 (ESM), we show possible compression factors (number of retained/original coefficients) for two threshold values and with respect to the original full matrix and to the block-diagonal filter matrix. However, in the latter case the advantage of thresholding depends on the smoothing effect of the filter and it certainly does not yield a very significant improvement. Consequently, we stick to the block-diagonal approach.

Figure 1 shows the filter coefficients $w(l, l', m, a)$ in logarithmic colorscale, row-wise for three different degrees a of smoothing (DDK1, DDK2, DDK3), column-wise for a selected number of harmonic orders m, and with l, l' on the horizontal/vertical axis of each single matrix plot for fixed m, a. Matrices in the figure are arranged for transforming a vector of coefficients with the minimum degree on top. Here $l_{\max}$ was set to 70. Noticeable are strong negative weights that couple (near-) sectorial GRACE coefficients with higher-degree filtered GRACE tesseral coefficients, and that are not at all mirrored by a symmetry property in the filter matrices. Our original intention was to fit analytical surfaces to the filter coefficients, i.e. to express the $w(l, l', m, a)$ as an analytic function of the variables l, l', m and a. This, however, turned out as difficult using standard methods such as low-degree polynomials, as the $w(l, l', m, a)$ do not behave in a rather 'regular' way (cf. Fig. 1). Therefore, instead of maintaining a large number of such expansion coefficients, we chose to simply store the original $w(l, l', m, a)$ in tables. These can be obtained on request (`roelof@gfz-potsdam.de`).

2.3. Data

The data for this study include 58 GFZ RL04 GRACE monthly solutions (Flechtner 2007), covering the time period 09/2002-08/2007 (missing months are 12/2002, 01/2003, 06/2003, 01/2004). In the processing of these solutions, the contributions of atmospheric and oceanic pressure variations, including ocean tides, were removed by applying background models. As a consequence, the monthly gravity fields represent mainly the direct and indirect (through loading) effect of land hydrologic variations such as large-scale groundwater and surface water level change. We define temporal variations δx_{lmq} by

removing the long-term average $\bar{x}_{lmq}$ of these fields. For the further investigations, two versions of these coefficient sets are generated. One set is expanded up to degree and order 70 and is then decorrelated using both the full matrix approach (Eq. (1)) and the order-convolution, block-diagonal approach. These coefficients are then synthesized to create models of surface mass variations (Eq. (2)) on a global grid. A second set of coefficients, to be used for the orbital tests, is decorrelated to obtain $\delta x^{\mathrm{filt}}_{lmq}$ up to degree and order 120. To these high-resolution filtered geopotential coefficients, the long-term average has been added back to allow for the orbit recovery based upon GRACE L1B data. This second set of coefficients is necessary to avoid aliasing signals that would map into the data residuals, as the L1B data (in particular the K-band) contains gravity information for degrees much beyond degree 70 (e.g., Gunter et al., 2006).

To this end, a degree/order 120 version of the DDK filters has been created. We have built a synthetic GRACE error covariance matrix as in Kusche (2007), i.e. using the GRACE twin-satellite orbital pattern of August 2003, but computing only the block-diagonal part. Then, employing the same power-law signal covariance model derived from models of ocean and land mass change, we built the optimal filter. Compared to the original approach using dense matrices, this technique results in a slightly different block-diagonal filter. The differences shown in table 4 (ESM) are sufficiently small, however.

For validation of our GRACE results we used a global land hydrology model: the Water Gap Hydrology Model (Döll et al, 2003). Original data is provided as the total monthly average water storage in mm units on a global $0.5^\circ \times 0.5^\circ$ grid, which we subsequently expand into spherical harmonics and refer to the long-term mean calculated in the same way

as we do with GRACE data. Expansion into spherical harmonic coefficients is performed by numerical integration. These coefficients are then converted to gravity potential coefficients by using the relation inverse to Eq. (2), and represented in the same form and units as the GRACE coefficients. The spherical harmonic sets can then be filtered by applying exactly the same mathematical operations as with GRACE data. The resulting sets can then be either mapped back into spatial grids or used to form basin averages.

3. Comparisons in terms of geopotential and surface mass changes

3.1. Fits at the GRACE observation level

Monthly GRACE gravity models are the outcome of a complex data reduction process, the current state of which is described e.g. in Flechtner (2007). An essential element of this process is a weighted least squares inversion, taking GRACE L1B data – inter-satellite K-band range rate (KRR) data, GPS code and phase tracking observations obtained from the two individual spacecraft – as input. The processing starts with an iterative precise orbit determination (POD) for the two spacecraft, relying on an *a priori* gravity model. KRR data is downweighted in the POD phase. The monthly spherical harmonic solutions provided to the public then follow from the last iteration of this process with reinstated KRR weighting. They are usually – apart from exceptional cases of data gaps and sparse coverage due to repeat orbital periods – unconstrained. This means that they, when used for generating synthetic GRACE observations, fit the true GRACE data in an optimal sense. Any constraining of the solution, be it by spectral truncation, direct regularization of the normal equation systems, or post-processing smoothing, is therefore expected to worsen this fit to some extent. The question that we investigate here is, whether our

decorrelated and smoothed gravity solutions ($\delta x^{\mathrm{filt}}_{lmq}$, of which only the time-variable part was postprocessed through the DDK filters) deteriorate the data fit significantly when compared to the least squares solution. Surprisingly, this kind of test appears to be performed for the first time here. We believe that the outcome of this evaluation helps to decide to what extent filtered (or otherwise constrained) GRACE solutions are reasonably justified by the original L1B data (which is the very data used to create the unconstrained solutions). It is worth mentioning that such an inspection of data fitting with respect to an adjustable degree of constraining has its recognized place in formal inversion theory (e.g. Parker, 1994); in particular, when searching for the 'optimal' degree of smoothing.

In order to save computation time, we have performed the test for GRACE orbit fits and observation residuals with decorrelated gravity models only for a single month, August 2003. Orbit determination was performed in all cases along the same (RL04) standards. As usual, KRR data are introduced with a sigma of $0.25\,{}^{\mu\mathrm{m}}/_{\mathrm{s}}$ (in the final step), GPS phase observations with a sigma of 0.85 cm and GPS code observations with a sigma of 35 cm (we use zero-differences of the ionosphere-free L3 combination for the GPS observables). In all cases, the decorrelated gravity models were introduced in the last step of the iteration and kept fixed (i.e. not adjusted any more).

Results from the POD phase are provided in table 5, where the numbers in brackets indicate the number of data points which passed our automatic (3sigma-) editing procedure. Somewhat unexpected, we find that the variation of the data fit RMS is in general very small, meaning that all considered fields fit the original data within close limits and none of them can be 'excluded' as unrealistic based on data misfit. With other words, the GRACE

L1B data permits – within some range – all solutions as realistic, which can qualitatively be explained through the ill-posedness of the problem. In addition to this, empirical orbit parameters are co-estimated for a best-possible POD that may absorb some gravity model differences. A closer inspection suggests that moderate decorrelation/smoothing (DDK3) slightly increases the number of accepted observations for the GPS data types. Similar results are found for KRR data residuals, cf. table 6. Decorrelation/smoothing appears to improve the fit RMS for KRR and GPS phase measurements slightly, but we believe the data fits are inconclusive here. It is possible that empirical KRR parameters (at the 1/rev frequency) absorb gravity model differences and thus tend to equalize the residual statistics. A deeper investigation is needed here, but we feel this is beyond the scope of this paper. When interpreting tables 5 and 6, one should also bear in mind that the number of accepted data does differ between solutions due to automatic editing (but much less than 1%), and that the shown RMS are not weighted. On the other hand, the original solution – including 'stripes' – fits as well as the decorrelated solutions. Hence, we can confirm that the 'striping' does not simply represent a geographical mapping of the data errors. It is more likely that small errors (most probably temporal aliasing from unmodelled short-period effects), cause small oscillations of the solutions, which are then amplified due to downward continuation.

3.2. Stability of basin specific periodic components

One of the most important GRACE applications is the determination of basin-specific mass change on smaller spatial scales, aiming at the validation and, eventually, calibration of hydrological modelling. In order to understand the potential influence of the postpro-

cessing procedures, the stability of periodic components detected in GRACE monthly solutions subjected to the different decorrelation filters (DDK1, DDK2, DDK3), was analyzed using the methodology described in Schmidt et al. (2008a).

As a preparatory step, the time series of the decorrelated GRACE solutions is transformed into space domain and converted into surface mass anomaly. To this set of monthly grids, Empirical Orthogonal Functions (EOF) analysis is applied, both to the data over all continents and to a number of selected water catchements. It should be noted that few modes explain the major part of the variability of the GRACE data (including signal and noise); e.g. in the Amazon basin the very first mode contains 77% (DDK1), 70% (DDK2), resp. 64% (DDK3), the first two 97% (DDK1), 94% (DDK2), resp. 88% (DDK3) of the total variability as derived from the GRACE RL04 models. The respective percentages for the Ganges basin are 94% (DDK1), 87% (DDK2), and 75% (DDK3) for the first mode, resp. 99% (DDK1), 96% (DDK2), and 88% (DDK3) for the sum of the first two. Comparing the principal components derived from different decorrelated models, we notice that leading modes vary only little (e.g. for DDK1 versus DDK3 the principle components of the first three modes of the Amazon are correlated by 1.00, 0.99, and 0.89. For Ganges, we find 0.99, 0.90, and 0.71.) With increasing mode number this difference becomes larger. Less smoothing causes higher modes to retain a larger amount of unsmoothed noise.

In a subsequent step, the principal components curves are subjected to a specific form of frequency analysis, which allows for finding arbitrary periods contained in data (cf. Petrovic et al. 2007, Schmidt et al. 2008a). The periods found in different principal components can then be sorted according to the part of variability of the original data

explained by them. In table 7 this is illustrated for some strong periods found in the basins of Amazon and Ganges. Using a Monte Carlo technique, in Schmidt et al. (2008a) we have shown that the formal (propagated) accuracy of the leading-mode phases and periods from GRACE can be as good as one day (i.e. $\sigma_\varphi \sim 1\,\text{day}$, $\sigma_T \sim 1\,\text{day}$) and better, whereas several (but not all) non-annual modes found in the data are much less well-determined.

In spite of the varying degrees of signal attenuation, resulting from the three applied decorrelation filters (compare Table 8 in ESM), the determination of periods and phases appears as very stable. Table 7 reveals that the majority of the period differences lies in a subday range, with only two exceptions. Regarding the longer periodic 2.1 year (763-772 days) wave found in Amazon, it should be taken into account that the determination of longer periodic variations from a time series with a time span of a few years only and monthly resolution must be less accurate (Schmidt et al., 2008a). The difference of 3.6 days for the 358 days cycle in Ganges can also be regarded as acceptable in view of monthly resolution of the data. The phase differences are somewhat larger, but still in the range of few days.

With respect to the determination of amplitudes, the well-known attenuation phenomena can be observed in Table 7. However, it should be noted that a 'stronger' filter does not attenuate the amplitudes of the dominant periodic terms as much as it attenuates the total signal. This is illustrated in table 8 (ESM) by the ratios of these amplitudes and the ratios of WRMS (area weighted root mean square), resulting from application of the filters DDK1-3. The dominant periodic terms describe the major part of the signal

variability. These terms cover in most basins more than 2/3 of the total signal content. Hence, the coherent basin-wide (leading periodic) signals are significantly less attenuated by a decorrelating filter compared to maps of the total (noise-contaminated) signal.

The results of this section point to the stable behavior of the considered decorrelation filters with respect to the characteristic features of temporal variability.

4. Comparisons in terms of global hydrology

As noted before, the major part of the variability contained in GRACE monthly fields over continents can be ascribed to water stock variations. Schmidt et al. (2008a, 2008b) provide a near complete survey of this type of research and the state of the art in hydrological applications of GRACE. Hydrological models have been the main source of validation for GRACE applications to hydrology. Therefore, for the filters discussed here we need to understand how filtered data sets behave with respect to these models. Specifically, we investigate how robust comparisons of GRACE with modelled hydrological variations are with respect to the applied smoothing parameter. To this end, WGHM surface mass anomaly maps over all continents (cf. section 2.3, all grid cells where WGHM has values) were smoothed using the same filters DDK as applied to GRACE.

First, the smoothed GRACE fields were evaluated by pointwise and global (over all continents) comparison against the smoothed hydrological model WGHM. Land maps of the surface mass WRMS from GRACE and from WGHM, and of the correlation coefficient between these two are shown in figures 2, 3, and 4 for decreasing smoothing. 'Stripes' in GRACE are only visible for DDK3 filtering, whereas DDK1 and DDK2 filters remove

them efficiently (cf. table 1 for corresponding Gaussian smoothing radius). From visual inspection, filtering affects WGHM much less than GRACE, with the exception of smaller regions with peak variablity. Weaker smoothing (DDK3) obviously leaves an unrealistically strong variability in GRACE.

Table 9 (ESM) provides a summary of the resulting global WRMS values and correlations. The last column displays correlations between GRACE and WGHM, which are relatively high. It is also visible that the correlation increases when the smoothing becomes stronger. From the WRMS values it follows that the signal variabilities contained in GRACE are stronger then those in WGHM, a fact noted by several researchers before (e.g. Tapley et al., 2004a, Schmidt et al., 2006, Güntner, 2008). However, from the ratios of WRMS values (table 9 in ESM) it appears that the attenuation factor for GRACE signals due to decorrelation rises more quickly with the increased smoothing than for WGHM signals (the WRMS ratio of 1.64 for DDK3 goes down to 1.47 for the stronger filter DDK1). This suggests that the filters damp striations more effectively than real signal.

Computing peak values of pointwise WRMS (per grid cell) yields the results displayed in Table 10 (ESM). The results in the last column are in contrast to those in Table 9 (ESM) discussed above. The attenuation of maxima for WGHM signals rises more quickly with the increased smoothing than for GRACE signals (the WRMS ratio of 1.12 for DDK3 goes up to 1.39 for the stronger filter DDK1. This indicates that some large-scale phenomena are missing in WGHM (or overestimated in GRACE) that are less affected by the filters. Visual inspections indeed confirms that the smoothed WGHM fields contain more variability at smaller spatial scales.

In addition, we provide a compilation of WRMS values from evaluating filtered GRACE solutions over regions, where we expect either large or almost negligible water mass change (table 11). We apply Gaussian filtering for comparison as well. For the Sahara, signals are indeed low (cf. also Fig. 2-4) and may be interpreted as a 'noise floor' for the particular solution. For the total ocean average, where the WRMS must be interpreted as the sum of the GRACE measurement error and the residual of the true ocean bottom pressure with respect to an *a priori* model removed in the GRACE de-aliasing processing, variability is somewhat larger compared to the Sahara. Amazon WRMS versus Sahara WRMS may thus well be understood as a signal/noise ratio, and it is distinctively larger for the DDK1 and DDK2 filters as compared to all Gaussian filters. It is obvious, but not surprising, that anisotropic filtering performs better in retaining large signals while suppressing what is believed to be noise.

5. Summary

We have analyzed recent GRACE GFZ RL04 monthly gravity solutions, using a new decorrelating post-processing approach. We find a very good agreement with mass anomalies derived from a global hydrological model (WGHM). The post-processed GRACE solutions exhibit relatively weak amplitude damping and almost negligeable phase shift and period distortion for relevant hydrological basins.

Furthermore, these post-processed GRACE solutions have been inspected in terms of data fit with respect to the original inter-satellite ranging and GPS observations. We find variations of the data fit owing to solution post-processing only within very narrow and nearly insignificant limits, confirming the suspicion that GRACE data does not 'pinpoint' the

standard unconstrained solutions too firmly.

Regarding our decorrelation and smoothing method, a simplified yet sufficiently accurate approach has been developed, which allows one to realize and use a higher resolution – as necessary for generating computed observations – and needs far less extra coefficients to be stored.

Acknowledgments. JK and RR acknowledge support provided by the German Research Foundation (DFG) under grant KU 1207/6-1, within the Special Priority Program SPP 1257 Mass Transport and Mass Distribution in the System Earth. RS and SP acknowledge support provided by the German Ministry of Education and Research (BMBF) and DFG within the geoscientific R+D program GEOTECHNOLOGIEN Erfassung des Systems Erde aus dem Weltraum under grant 03F0424A. We thank P. Döll for providing WGHM model data, U. Meyer for help with the GRACE SLR/GPS/KRR statistics, D. W. Pierce for his EOF software, and three anonymous reviewers for helpful remarks.

References

Chambers D., Wahr J., Nerem R. S. (2004), Preliminary observations of global ocean mass variations with GRACE, Geophys. Res. Lett., 33., doi:10.1029/2004GL020461

Colombo O. L. (1986), Notes on the mapping of the gravity field using satellite data. In: H. Sünkel, ed., Mathematical and Numerical Techniques in Physical Geodesy, Lecture Notes in Earth Sciences, vol. 7, Springer, Berlin

Davis J., Tamisea M., Elósegui P., Mitrovica J., Hill E. (2008), A statistical filtering approach for Gravity Recovery and Climate Experiment (GRACE) gravity data Journal

of Geophysical Reaseach – Solid Earth, 113, B04410, doi:10.1029/2007JB005043

Döll P., Kaspar F., Lehner B. (2003), A global hydrological model for deriving water availability indicators: model tuning and validation, J. Hydr. 270(1-2):105-134.

Fenoglio-Marc L., Kusche J., Becker M. (2006), Mass variation in the Mediterranean Sea and its validation by altimetry, steric and hydrologic fields, Geophys. Res. Lett., 33., doi:10.1029/2006GL026851

Flechtner F. (2007), GFZ Level-2 processing standards document for level-2 product release 0004, GRACE 327-743, Rev. 1.0

Güntner A. (2008), Improvement of global hydrological models using GRACE data, Surveys in Geophysics, doi:10.1007/s10712-008-9038-y

Gunter B., Ries J., Bettadpur S., Tapley B., (2006), A simulation study of the errors of omission and commission for GRACE RL01 gravity fields, Journal of Geodesy, doi:10.1007/s00190-006-0083-3

Han S.-C., Simons F., (2008), Spatiospectral localization of global geopotential fields from the Gravity Recovery and Climate Experiment (GRACE) reveals the coseismic gravity change owing to the 2004 Sumatra-Andaman earthquake, Journal of Geophysical Reaseach – Solid Earth, 113, B01405, doi:10.1029/2007JB004927

Klees R., Revtova E., Gunter B., Ditmar P., Oudman E., Winsemius H., Savenije H. (2008), The design of an optimal filter for monthly GRACE gravity models, Geophys. J. Int., doi:10.1011/j.1365-246X.2008.03922.x

Kusche J. (2007), Approximate decorrelation and non-isotropic smoothing of time-variable GRACE-type gravity field models, J. Geod. 81:733-749, doi:10.1007/s00190-007-0143-3

Parker R. L. (1994), Geophysical Inverse Theory, Princeton University Press, New Jersey

Petrovic S., Schmidt R., Wünsch J., Barthelmes F., Güntner, A., Rothacher, M. (2007), Towards a characterization of temporal gravity field variations in GRACE observations and global hydrology models, Proceedings of the 1st International Symposium of the International Gravity Field Service, Gravity Field of the Earth, Istanbul, General Command of Mapping, Journal of Mapping (ISSN 1300-5790), Special Issue: 18, pp. 199-204.

Schmidt R., Schwintzer P., Flechtner F., Reigber C., Güntner A., Döll P., Ramillien G., Cazenave A., Petrovic S., Jochmann H., Wünsch J. (2006), GRACE observations of changes in continental water storage, Global and Planetary Change, 50(1-2):112-126

Schmidt R., Petrovic S., Güntner A., Barthelmes, F., Wünsch, J., Kusche, J. (2008a), Periodic components of water storage changes from GRACE and global hydrology models, Journal of Geophysical Reaseach – Solid Earth, doi:10.1029/2007JB005363

Schmidt R., Flechtner F., Meyer U., Neumayer K.-H., Dahle C., König R., Kusche J. (2008b), Hydrological signals observed by the GRACE satellites, Surveys in Geophysics, doi:10.1007/s10712-008-9033-3

Swenson S. and Wahr J. (2006), Post-processing removal of correlated errors in GRACE data, Geophys. Res. Lett., 33, L08402, doi:10.1029/2005GL025285

Swenson S. and Wahr J. (2007), Multi-sensor analysis of water storage variations in the Caspian Sea, Geophys. Res. Lett., 34, L16401, doi:10.1029/2007GL030733

Tapley B., Bettadpur S., Ries J., Thompson P., Watkins, M. (2004a), GRACE measurements of mass variability in the Earth system, Science, 305, 503-505

Tapley B., Bettadpur S., Watkins, M., Reigber C. (2004b), The gravity recovery and climate experiment: Mission overview and early results. Geophys. Res. Lett., 31, L09607, doi:10.1029/2004GL019920

Wahr J., Molenaar M., Bryan F. (1998), Time variability of the Earth's gravity field: Hydrological and oceanic effects and their possible detection using GRACE, Journal of Geophysical Reaseach – Solid Earth, 108(B12):30,205-30,229

Wouters B. and Schrama E.J.O. (2007), Improved accuracy of GRACE gravity solutions through empirical orthogonal function filtering of spherical harmonics, Geophys Res Lett, 34, L23711, doi:10.1029/2007GL032098

Velicogna I. and Wahr J. (2006), Measurements of time-variable gravity show mass loss in Antarctica, Science 311, 1754

	Corresponding Gaussian radius (km)		parameter a and p
decorrelation filter	acc. to Kusche (2007, tables 1+2)	acc. to $\omega_l = \frac{1}{2}$	acc. to Kusche (2007)
DDK1	1350	530	$a = 1 \cdot 10^{14}$, $p = 4$
DDK2	900	340	$a = 1 \cdot 10^{13}$, $p = 4$
DDK3	660	240	$a = 1 \cdot 10^{12}$, $p = 4$

Table 1. Smoothing characteristics of the three decorrelation filters used in this study. The parameter a is a weighting factor. By p we denote the exponential parameter in a power law of the type l^{-p}, fitted to the empirical signal degree variance (for details, cf. Kusche 2007, Eq. (47) and (48)).

decorr. filter	max. off-b.d. entry	min. off-b.d. entry	max. mixed-parity entry	min. mixed-parity entry	max. mixed-trig. entry	min. mixed-trig. entry
DDK1	0.010	−0.012	0.020	−0.017	0.003	−0.005
	$w^{18;18;0}_{3;3;1}$	$w^{11;11;1}_{4;4;0}$	$w^{24;2;0}_{23;2;0}$	$w^{34;3;1}_{3;3;1}$	$w^{17;15;0}_{15;15;1}$	$w^{17;15;1}_{17;15;0}$
DDK2	0.009	−0.011	0.027	−0.013	0.002	−0.007
	$w^{21;21;0}_{6;6;1}$	$w^{19;18;0}_{13;12;1}$	$w^{34;3;1}_{33;3;1}$	$w^{40;5;0}_{5;5;0}$	$w^{19;15;0}_{15;15;1}$	$w^{16;15;0}_{16;15;1}$
DDK3	0.011	−0.012	0.035	−0.009	0.009	−0.006
	$w^{42;36;1}_{30;25;1}$	$w^{31;30;1}_{16;15;0}$	$w^{44;45;1}_{44;4;1}$	$w^{46;9;1}_{9;9;1}$	$w^{2;0;1}_{70;0;0}$	$w^{39;15;1}_{39;15;0}$

Table 2. **(ESM)** Maximum deviations for the three filters from the properties of Eq. (6) and Eq. (7), $l_{\max}$=70. 'Off-b.d.' refers to Eq. (6), third line. 'Mixed-parity' refers to Eq. (6), fourth and fifth line. 'Mixed-trig.' refers to Eq. (6), first line, for $m = m'$.

	compression w.r.t.			
decorrelation filter	full mat.		b.-d. mat.	
	$\varepsilon = 0.01$	$\varepsilon = 0.001$	$\varepsilon = 0.01$	$\varepsilon = 0.001$
DDK1	0.00017	0.00045	0.07	0.19
DDK2	0.00031	0.00079	0.13	0.33
DDK3	0.00052	0.0012	0.22	0.51

Table 3. **(ESM)** Compression factors for the three filters with thresholding, with respect to full or block-diagonal representation, $l_{\max}$=70

decorrelation filter	Entry	max. diff.	rel. diff. %	Full	b.-d.
DDK1	$w^{35;30;1}_{35;30;1}$	0.0012	0.4	0.288	0.289
DDK2	$w^{19;18;0}_{19;18;0}$	0.0007	0.2	0.415	0.416
DDK3	$w^{17;15;1}_{17;15;1}$	0.0004	0.2	0.196	0.196

Table 4. **(ESM)** Maximum differences of block diagonal filter with respect to full matrix filter, $l_{\max}$=70

decorrelation filter	SLR RMS (cm)	GPS code RMS (cm)	GPS phase RMS (cm)
DDK1	4.96 (4108)	35.72 (1096407)	0.556 (1096407)
DDK2	4.95 (4108)	35.72 (1096441)	0.554 (1096441)
DDK3	4.94 (4108)	35.75 (1096765)	0.555 (1096765)
no decorrelation	4.95 (4108)	35.74 (1096636)	0.554 (1096636)

Table 5. Data fits (SLR residuals, GPS code and phase residuals) from original and decorrelated GRACE solutions ($L = 120$). In brackets () the number of data points after automatic editing.

decorrelation filter	KRR RMS (μm/s)
DDK1	0.3125 (485698)
DDK2	0.3126 (485741)
DDK3	0.3137 (485935)
no decorrelation	0.3139 (484170)

Table 6. Data fits of Kband range rate residuals from original and decorrelated GRACE solutions ($L = 120$). In brackets () the number of data points after automatic editing.

		DDK1			Δ period		ampl. ratio		Δ phase	
		period	ampl.	phase	DDK2-1	DDK3-1	$\frac{\text{DDK2}}{\text{DDK1}}$	$\frac{\text{DDK3}}{\text{DDK1}}$	DDK2-1	DDK3-1
	mode	(days)	(-)	(days)	(days)	(days)	(-)	(-)	(days)	(days)
Amazon	1	361.9	7.63	114.3	0.1	-0.0	1.09	1.12	1.0	3.0
	2	361.5	3.73	201.3	0.3	0.4	1.27	1.35	1.6	3.4
	3	772.4	0.50	75.1	-5.0	-9.7	1.64	2.02	-15.3	-5.9
	1	459.6	0.90	469.8	0.1	0.6	1.22	1.27	1.7	4.8
Ganges	1	365.2	2.88	264.4	0.1	0.0	1.12	1.16	-0.5	-3.1
	1	184.8	0.76	60.3	-0.1	-0.6	1.11	1.09	-2.0	-4.6
	2	358.3	0.47	355.8	0.5	3.6	1.85	2.55	-1.9	-1.7

Table 7. Period, amplitude and phase of the most dominant periodic features for the Amazon and Ganges basins resulting from principal components of GRACE monthly solutions, as seen by the decorrelation filters; periods and phases in days, amplitudes in relative units (in our convention, EOF's have units of mm).

	DDK2/DDK1		DDK3/DDK1	
	WRMS	amplitude	WRMS	amplitude
Amazon	1.15	1.09	1.23	1.12
Ganges	1.20	1.12	1.36	1.16
Niger	1.23	1.20	1.48	1.32
Volga	1.11	1.01	1.36	0.99

Table 8. (ESM) Comparison of the damping of WRMS and of the amplitude of the most dominant periodic feature for four large water catchements when applying different decorrelation filters to GRACE monthly solutions

decorrelation	GRACE WRMS		WGHM WRMS		WRMS ratio	correlation
filter	(cm)	relative	(cm)	relative	GRACE/WGHM	GRACE-WGHM
DDK1	5.89	1.00	4.01	1.00	1.47	0.79
DDK2	7.03	1.19	4.72	1.17	1.49	0.74
DDK3	8.58	1.45	5.23	1.30	1.64	0.62

Table 9. (ESM) Comparison of decorrelated GRACE fields with filtered WGHM hydrology model: WRMS in cm and relative units (w.r.t. DDK1), ratios of WRMS-values and correlations between GRACE and WGHM; computed from 58 monthly solutions (2002/08-2007/09) using all pixels over all continents

	GRACE			WGHM			
decorrelation	absolute		relative	absolute		relative	ratio MAX
filter	MIN	MAX	MAX	MIN	MAX	MAX	$\frac{\text{GRACE}}{\text{WGHM}}$
DDK1	1.17	20.96	1.00	0.17	15.04	1.00	1.39
DDK2	1.66	26.16	1.25	0.18	21.93	1.46	1.19
DDK3	3.21	32.49	1.54	0.14	28.99	1.92	1.12

Table 10. (ESM) MIN/MAX (in cm) of pixel-wise WRMS for GRACE and WGHM over all continents, MAX also in relative units (w.r.t. DDK1) and as ratios GRACE/WGHM

	GRACE WRMS					
	DDK1	DDK2	DDK3	Gauss (530 km)	Gauss (340 km)	Gauss (240 km)
Global	3.87	4.77	6.46	3.99	7.54	35.77
Continents	5.89	7.03	8.58	5.78	8.97	35.30
Ocean	2.66	3.44	5.33	3.02	6.94	36.25
Amazon	14.34	16.47	17.66	13.32	16.73	41.75
Sahara	1.75	2.56	4.82	2.46	6.56	35.55

Table 11. Pixel-wise WRMS (in cm) for GRACE as seen by the three decorrelation filters and by Gaussian filters. Evaluated globally, for the total continent and ocean surface, and for the Amazon and Sahara regions.

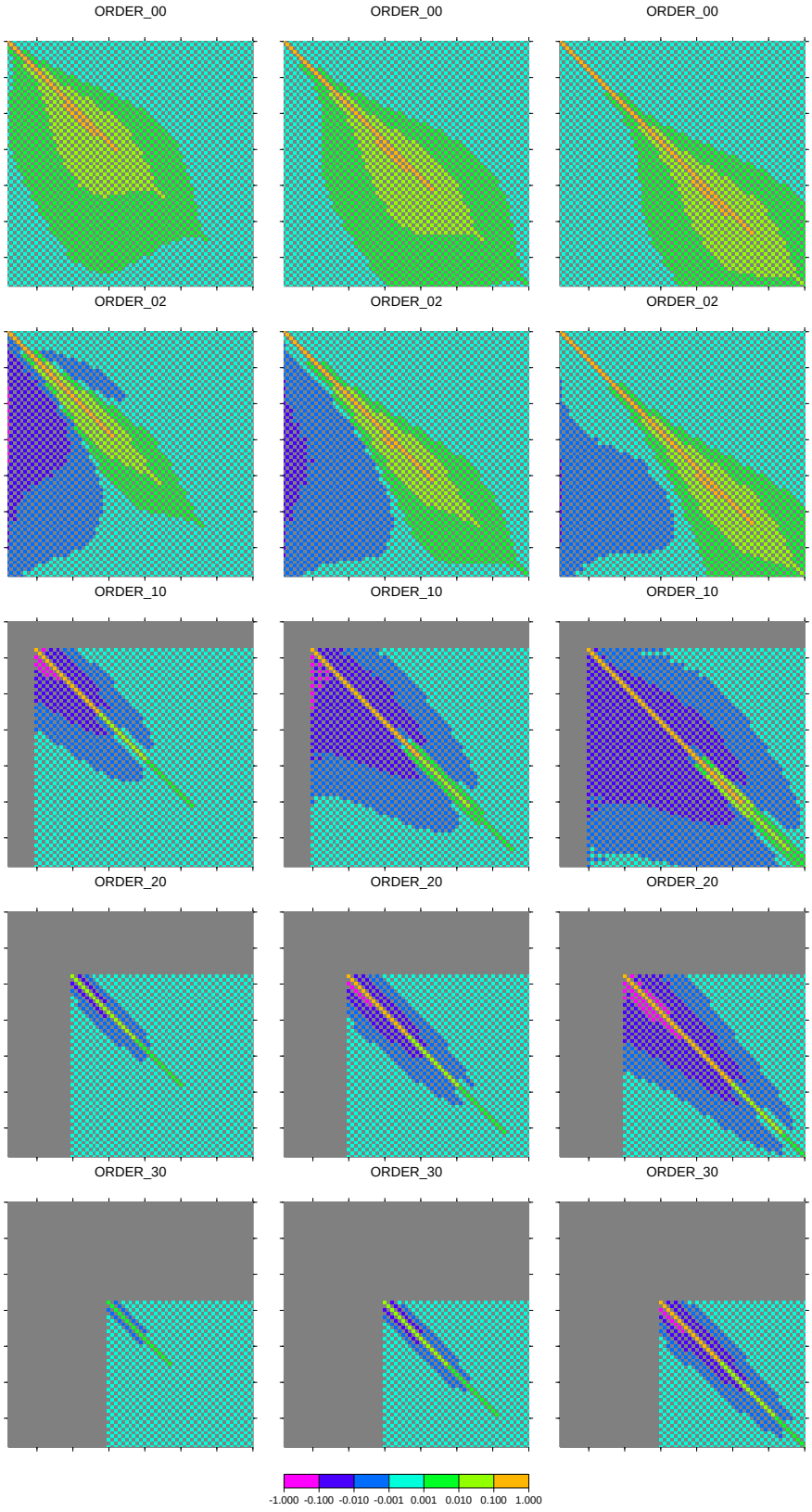

Figure 1. Coefficients $w(l, l', m, a)$ for m as in the figure headers, decorrelation filters DDK1 (left), DDK2 (middle), DDK3 (right)(cf. table 1)

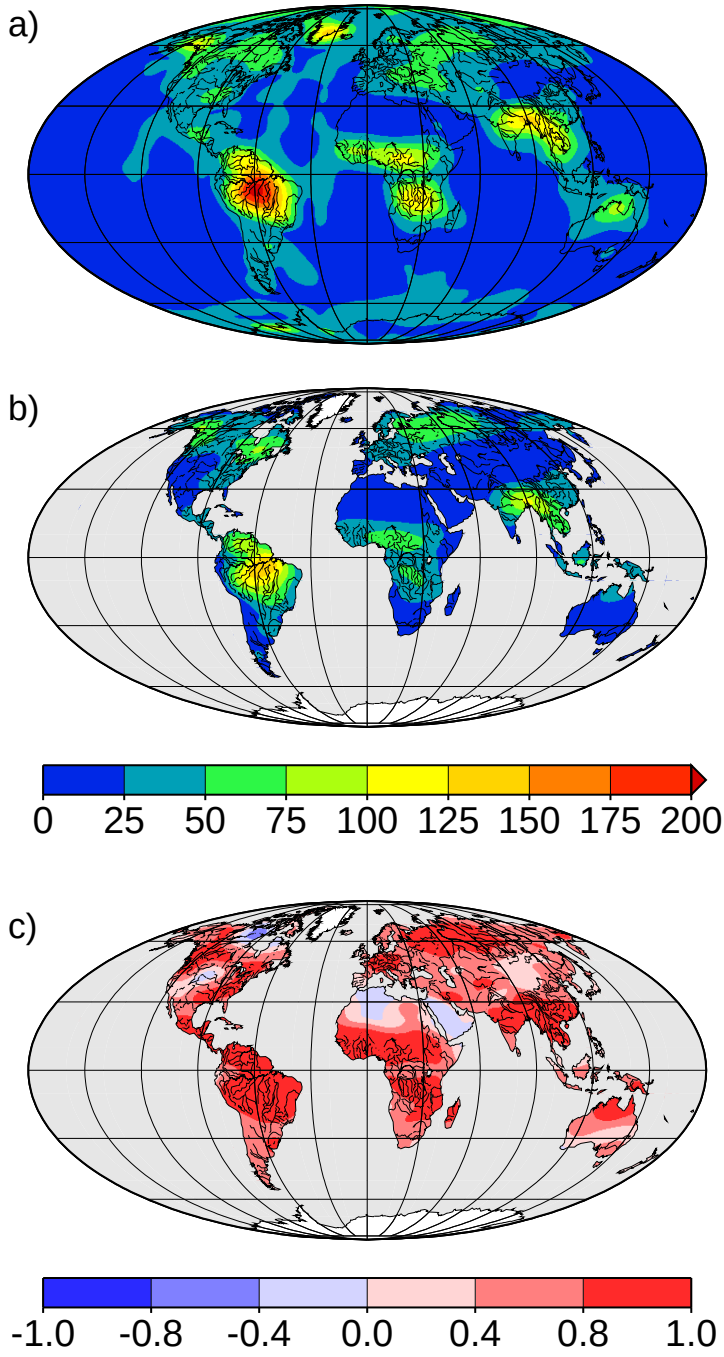

Figure 2. Pixel-wise WRMS of GRACE (a) and WGHM (b), both in mm, and the pixel-wise correlation of GRACE and WGHM (c), as seen by the decorrelation filter DDK1

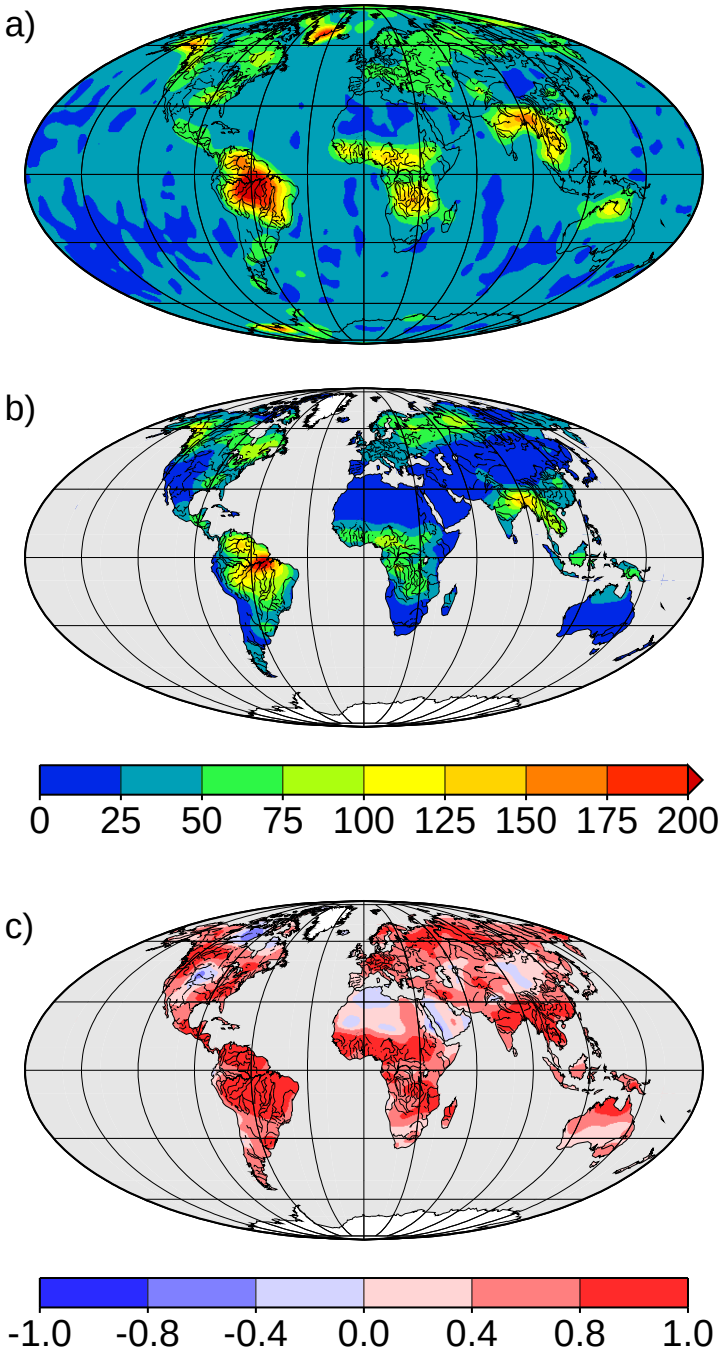

Figure 3. Pixel-wise WRMS of GRACE (a) and WGHM (b), both in mm, and the pixel-wise correlation of GRACE and WGHM (c), as seen by the decorrelation filter DDK2

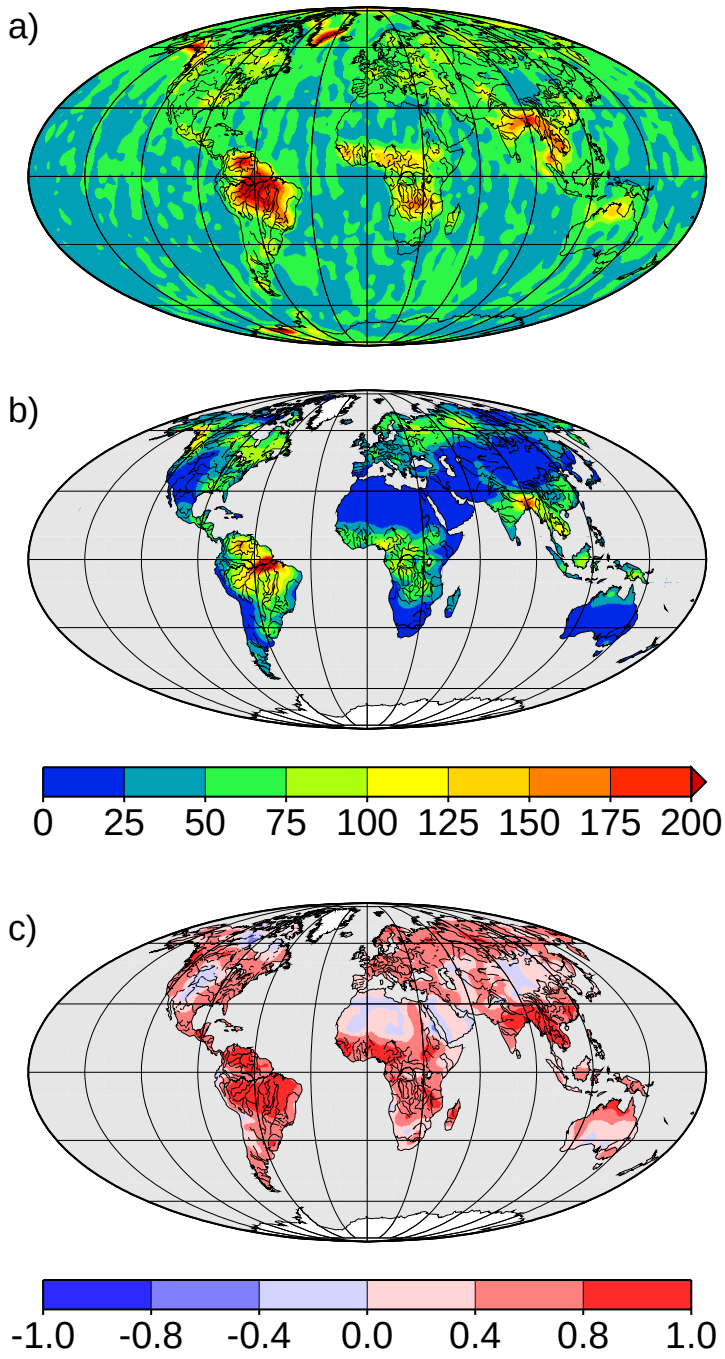

Figure 4. Pixel-wise WRMS of GRACE (a) and WGHM (b), both in mm, and the pixel-wise correlation of GRACE and WGHM (c), as seen by the decorrelation filter DDK3

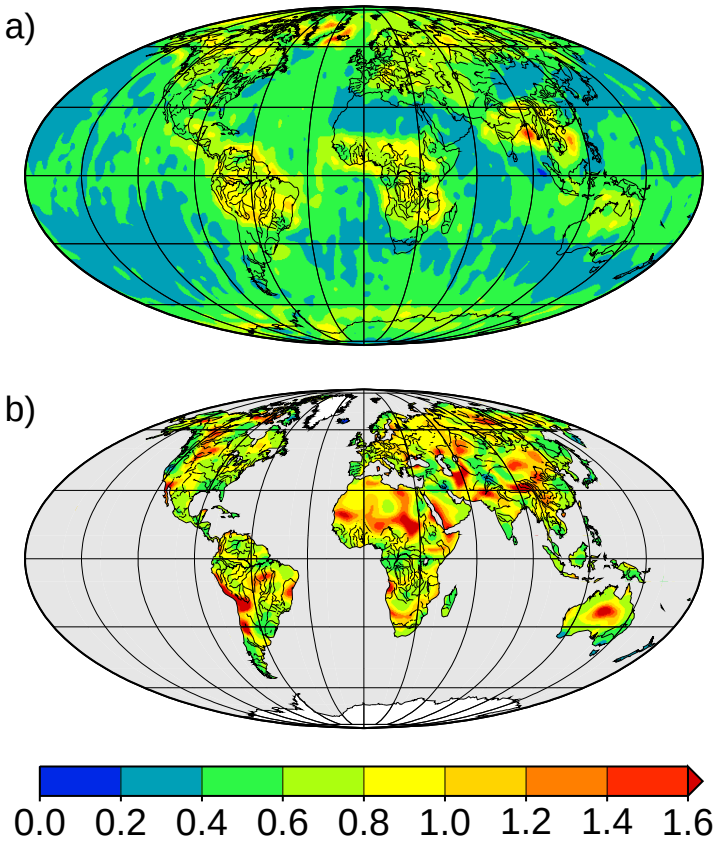

Figure 5. Ratios of pixel-wise WRMS for two decorrelation filters (DDK3/DDK1) for GRACE (a) and WGHM (b)